INTERFEROMETRIC MULTI-CHROMATIC ANALYSIS OF HIGH RESOLUTION X-BAND DATA

F. Bovenga[1], V. M. Giacovazzo[1], A. Refice[1], D.O. Nitti[2], N. Veneziani[1]

[1] *CNR-ISSIA, via Amendola 122 D, 70126 Bari, Italy, E-mail: bovenga@ba.issia.cnr.it*
[2] *Dipartimento Interateneo di Fisica, Politecnico di Bari, via Amendola 173, 70126 Bari, Italy, E-mail: davide.nitti@fisica.uniba.it*

ABSTRACT

The Multi-Chromatic Analysis (MCA) consists of performing sub-bands splitting in range frequency domain, thus generating chromatic views of lower range resolution, centered at different carrier frequencies. Multi-chromatic interferograms can be then generated by coupling chromatic views coming from an interferometric pair of SAR images. The interferometric phase of spectrally-stable scatterers evolves linearly with the sub-band central frequency, the slope being proportional to the absolute optical path difference. Unlike the standard "monochromatic" InSAR approach, this new technique allows performing spatially independent and absolute phase unwrapping (PU). Potential applications for the study of spectrally-stable targets include topographic measurements, atmospheric research or urban monitoring.

The technique appears optimally suited for new-generation, wide-band, high-resolution satellite SAR sensors. This work presents first successful applications of the technique using both TerraSAR-X (TSX) and COSMO/SkyMed (CSK) spotlight data. In particular, we provide results concerning the use of MCA for performing absolute PU as well as for height measurement on a pixel-by-pixel basis. Moreover, the impact of coregistration procedure on the MCA-based inference is investigated.

1. INTRODUCTION

The Multi-Chromatic Analysis, as introduced in [1], uses interferometric pairs of SAR images processed at range sub-bands and explores the phase trend of each pixel as a function of the different central carrier frequencies. The phase of stable scatterers evolves linearly with the sub-band central wavelength, the slope being proportional to the absolute optical path difference. Unlike the standard "monochromatic" InSAR approach, this new multi-chromatic technique allows performing spatially independent and absolute topographic measurements, if the attention is focused on single targets exhibiting stable phase behaviour across the frequency domain. Potential applications for the study of frequency-stable targets include topographic measurement, atmospheric research, and urban monitoring.

Through a simplified model [2], we obtained a first evaluation of the impact of the MCA processing parameters on the height estimation performances. Results showed that the estimation is improved by using wider bandwidths for the sub-look images, and by increasing the number of sub-looks. Moreover, a total bandwidth of at least 300 MHz seems to be required to provide reliable results. Thus, the technique appears optimally suited for the new generation of satellite sensors, which operate with larger bandwidths than previously available instruments, generally limited to few tens of MHz. SAR sensors such as those mounted on TSX or CSK spacecraft, all pose great expectations on the potential use of multi-chromatic methods.

The practical feasibility of the technique was demonstrated in past [2] by using a set of SAR data collected by the airborne AES-1 radar interferometer, operating at X-band by multi-channel electronics, which provides a total radar bandwidth of 400 MHz. In the present work we illustrate MCA processing on spaceborne SAR data acquired by the TSX mission, as well as by the CSK constellation. Both datasets satisfy the processing requirements derived from the theoretical modelling and the prototype processing of the AES-1 dataset [2]. A first successful application of the technique to satellite data was already shown in [3] by using a TSX dataset. Here, we show results obtained by processing also CSK data. Moreover, we investigate the impact of coregistration procedure on the MCA-based inference.

Section 2 summarizes MCA principles relevant to the experiment. In section 3 we show the application of MCA for performing PU as well as for absolute height measurement by using both TSX and CSK data. Finally, we provide comments and conclusions.

2. MCA PRINCIPLES

The main steps in the MCA processing are: i) the generation of N_i sub-looks for both master and slave images, by splitting the whole range band into N_i narrower sub-bands, centered at different frequencies (f_i); ii) the generation of a stack of N_i interferograms

computed by coupling equivalent master and slave sub-look images; iii) a pixel-by-pixel linear regression, performed on the wrapped interferometric phase samples at different frequencies, according to the following relationship [2]:

$$\Phi_i^W(x,r) = -2\pi \cdot k(x,r) - \frac{4\pi}{c} \cdot \Delta R(x,r) \cdot f_i = \qquad (1)$$
$$= C_0(x,r) + C_1(x,r) \cdot f_i$$

Since the slope coefficient C_1 is related to the range difference between master and slave, it can be used to compute on a pixel-by-pixel basis the absolute phase, and consequently to perform PU:

$$\Phi^{UW}(x,r) = C_1(x,r) \cdot f_c \qquad (2)$$

where f_c is the carrier frequency of the original full-band images.

An a posteriori estimation of the multi-frequency phase error σ_ϕ is given by the root mean square difference between the interferometric phases measured at the different frequencies f_i, and the corresponding values computed by the linear model. This quantity defines an inherent inter-band coherence for the MCA and can be assumed as a quality index of the measurements. Frequency coherent pixels can be selected as: $PS_{fd} = \{(x,r) \mid \sigma_\phi(x,y) \le \sigma^{th}_\phi\}$.

The MCA processing chain has been designed to have in input a pair of SLC images already co-registered, to avoid increasing computational efforts related to the co-registration between master and slave images for each sub-bands. When the sub-bands filtering is applied to the slave image already co-registered, an additional phase term arises in the sub-band images, which is proportional to the sub-band frequency and to the range shift $\Delta R_{sh}(x,y)$ applied pixel by pixel during co-registration. Thus, by taking into account this term, Eq. 2 becomes:

$$\Phi^{UW}(x,r) = \left[C_1(x,r) - \frac{4\pi}{c} \Delta R_{sh}(x,r) \right] \cdot f_c \qquad (3)$$

The coregistration shift compensation can be performed after the slope estimation, together with the removal of the reference phase contribution. This approach is advantageous also with respect to the constraint on the spacing between the sub-bands, needed to avoid phase aliasing along the frequency domain. Since ΔR is decreased by a factor ΔR_{sh}, the maximum distance between adjacent sub-frequencies is increased of the same amount, thus slightly relaxing the constraints on the number of sub-bands to be processed. The range shift matrix $\Delta R_{sh}(x,y)$ also provides a coarse estimation of the path difference between master and slave, and is usually obtained through amplitude cross-correlation

[4]. The amplitude of a SAR image depends on the geometry of the satellite view, but it is less sensitive than the interferometric phase. Therefore the inference of the range shift based on the amplitude correlation requires high baseline values in order to provide reliable accuracy: it is the principle of radargrammetry, which is performed by using high parallax (baseline) values.

In the following, we use MCA for performing PU as well as for absolute height measurement. In particular, we verify the presence of different contributions to the height measurement coming from both the co-registration shifts as well as the phase analysis along the frequencies (provided by the MCA):

$$H(x,y) \approx \Phi 2H \cdot \left(\Phi^{UW}(x,r) - \Phi^{ref}(x,r) \right)^{(3)} = \qquad (4)$$
$$= H_{MCA}(x,y) + H_{shift}(x,y)$$

where $\Phi 2H$ is a coefficient which transforms absolute phase into height, and $\Phi^{ref}(x,r)$ is the InSAR phase relative to an ellipsoidal model of the Earth surface. Both $\Phi^{ref}(x,r)$ and $\Phi 2H(x,r)$ are computed during standard InSAR pre-processing, according to the relative position between the sensor and the ground.

3. AYERS ROCK TEST CASE

The Ayers Rock dataset consists of two images acquired by the TSX satellite over Ayers Rock (Australia) in spotlight mode. The full bandwidth of 300 MHz guarantees the applicability of MCA processing [2]. On the left side of Tab. 2, relevant parameters of this dataset are listed. In Fig. 1, the footprint of the SAR acquisition is shown in magenta, superimposed over an optical image extracted from Google-Earth. The white borders enclose the area selected for the experiment which covers both part of the flat plateau as well as the top of the monolith that stands about 320 meters high.

This rock formation presents strong terrain slopes that cause layover and shadow effects clearly visible in the SAR amplitude image (see Fig.2-(A)). The land coverage is mainly bare, leading to low temporal decorrelation.

Table 1. Relevant parameters for TSX dataset (left) and CSK dataset (right)

TerraSAR-X dataset	COSMO/SkyMed dataset
• Spotlight	• Spotlight
• Slave: 12.02.2009	• Master: 18.09.2010
• Master: 23.02.2009	• Master: 19.09.2010
• Bn = - 233.100m	• Bn = 112 m
• Bp = - 209.54m	• Bp = 75 m
• fo = 9.65 GHz (λ=3.11 cm)	• fo = 9.6 GHz (λ=3.12 cm)
• B = 300 MHz	• B = 379 MHz
• Slant range res. = 0.5 m	• Slant range res. = 0.5 m
• Azimuth res. = 1.1 m	• Azimuth res. = 1.1 m
• Ha ~ 34 m	• Ha ~ 44 m

Figure 1. Ayers Rock test site. The footprint of the SAR acquisition is shown in magenta, superimposed over an optical image extracted from Google-Earth. The white borders enclose the area selected for the experiment. The bottom picture reports the estimated height of the plateau.

A Digital Elevation Model (DEM) derived from SRTM mission is available on the same area. The DEM has a resolution of 90x90 m^2 and has been resampled onto the SAR geometry to allow direct comparison wrt the products derived by MCA.

A classical interferometric processing was performed at full band without using the DEM-assisted co-registration procedure in order to point out possible effects of local mis-registration errors and, consequently, the contribution of the MCA in the height reconstruction. Then, the co-registered images were processed through the MCA algorithm, using 23 sub-bands of 60 MHz each, thus spanning a total frequency range of 226.7 MHz. Themap of the $C_1(x,y)$ slope factor, and that of the quality index $\sigma_\phi(x,y)$, are then computed through linear regression. The absolute phase derived by MCA was computed through Eq. (3), by also taking into account the contribution coming from the shift along range applied during co-registration.

Fig. 2 shows both the absolute phase (inset B) as well as the absolute phase after the reference phase removal (inset C). The latter shows clearly two different phase values related respectively to the plateau and to the top of the monolith.

We filtered this absolute interferometric phase measurements by using a mean filter, to derive a smooth continuous phase surface, with phase jumps from one pixel to its neighbour lower than half a cycle. This smoothed absolute phase measurement was then wrapped modulo-2π to show the corresponding interferogram. The resulting fringe pattern is shown in Fig. 2-(D) for comparison with the original one in Fig.2-

(E). Even though the interferogram derived from the smoothed phase is noisy, the same structure is clearly observable in both interferograms. Moreover, the number of fringes on the monolith as also their shape appears quite well preserved. To verify this statement, we used the smoothed absolute interferometric phase to flatten the classical interferogram. The result, shown in Fig. 2-(F), is a phase field with values contained within $\pm 2\pi$, which means that the smoothed absolute phase surface is a correct unwrapped version of the classical interferogram within less than a cycle.

The aim of this experiment is, in particular, to verify the different contributions to the height measurement coming from both the co-registration shifts (in case co-registration is performed once, before splitting) and from the phase analysis along the frequencies (provided by the MCA).

Once the unwrapped phase has been validated, we computed the height map in Eq. (4).

Fig. 3 shows the maps of H_{MCA}, H_{shift} and H in the insets (A), (B) and (C), respectively. For comparison, the height H_{SRTM} derived by resampling the SRTM DEM onto the SAR geometry is sketched in the inset (D) of the same figure. By looking at the map of the heights derived from the co-registration shifts, it is evident that the elevation of the top of the monolith w.r.t. the flat plateau stays well below the expected value, which is about 320 m (see H_{SRTM}). The histogram in Fig.3-(E) epresents the difference between H_{shift} and H_{SRTM} and clearly shows two peaks: one around −283 m, which refers to a global offset on the height measurement, and a second one which is related to the error in the height values measured on the top of the monolith. This error is basically due to the fact that we used a co-registration procedure not supported by an external DEM, which can fail in presence of steep slopes, as is the case along the monolith flanks.

The elevation map in Fig.3-(A) was derived by using the C_1 map computed by the MCA processing, followed by a spatial mean filtering, needed to reduce the noise level and to obtain an almost continuous surface. This MCA-based heights map is able to correct (except for a bias) the height profile derived from the co-registration shift, as can be proved by looking at the elevation map H computed through Eq. (4). The histogram of the difference between H and H_{SRTM} is sketched in Fig. 3-(F): the peak related to the error in the height values measured on the top of the monolith disappears. The differences are still peaked at a non-zero value, meaning that a global offset is present. This offset can be explained in term of both artefacts induced by the atmosphere, and inaccuracies in the orbital parameters. A first assumption in performing absolute height measurements is that phase artefacts due to the atmosphere are either negligible or properly estimated and removed.
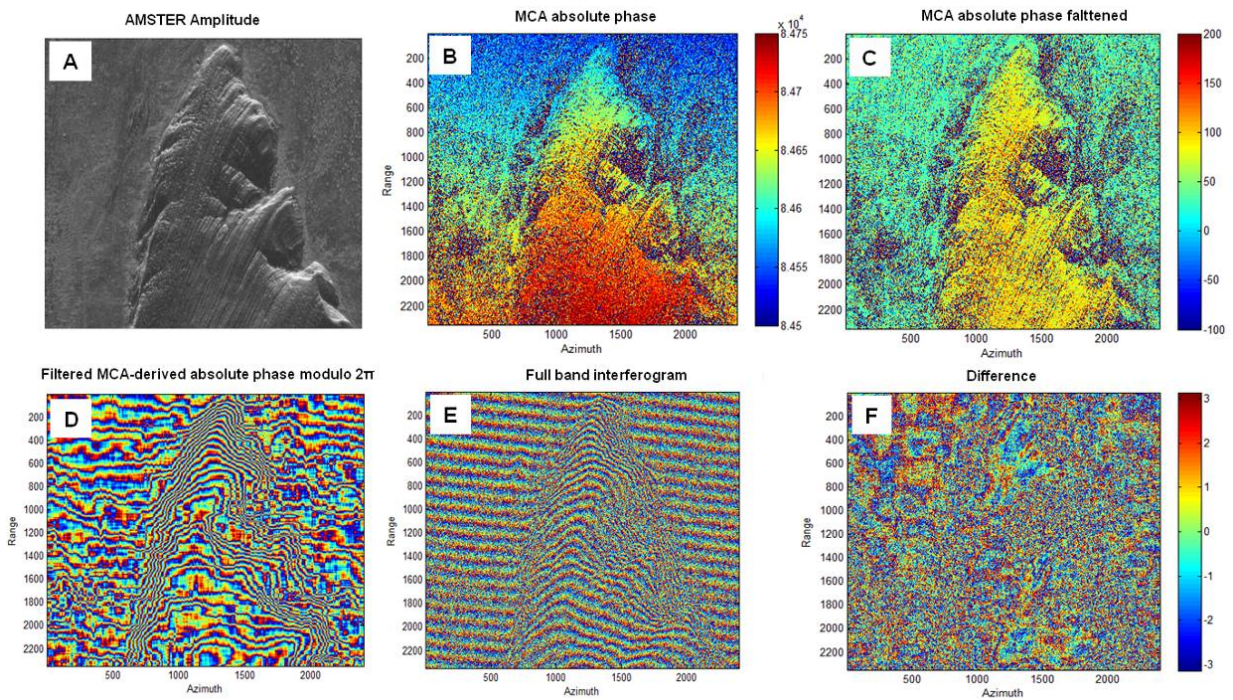
Figure. 2 (A) Amplitude of the master images. (B) MCA-based absolute phase. (C) MCA-based absolute phase after the reference phase removal. (D) Fringe pattern derived from absolute phase in inset (B). (E) Fringe pattern of the full band interferogram. (F) Full-band interferogram flattened by using the MCA-based absolute phase.
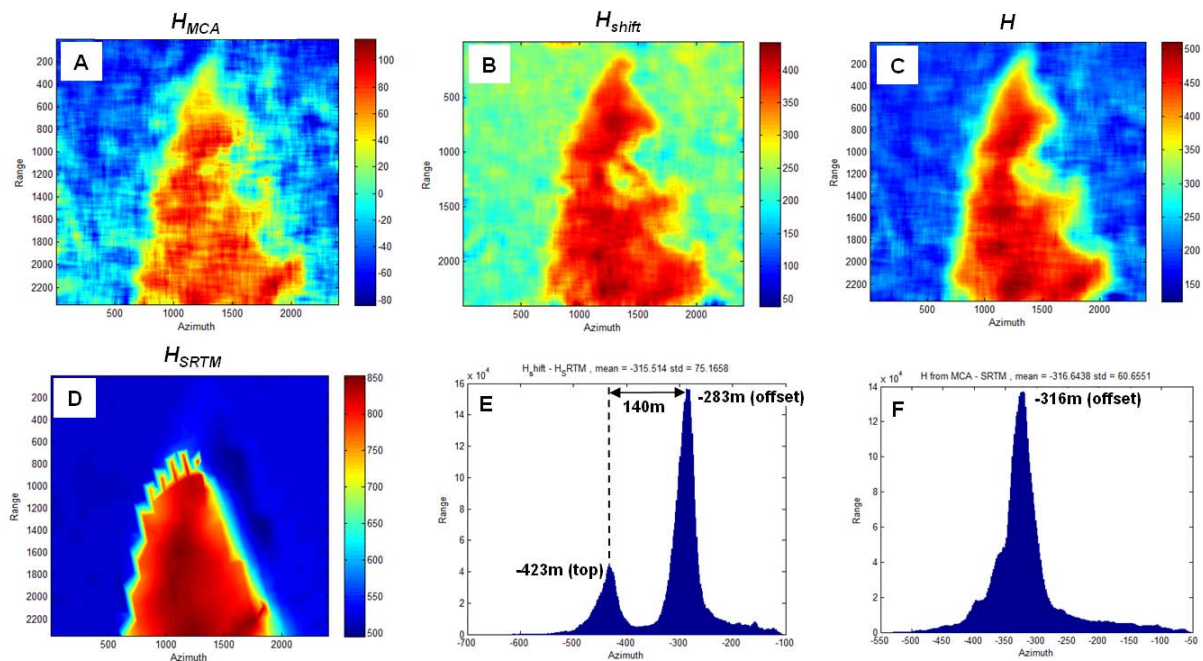

Figure. 3 Maps of H_{MCA}, H_{shift} and H are swhon in the insets (A), (B) and (C), respectively. (D) Heights derived by resampling the SRTM DEM onto the SAR geometry. (E) Histogram of the difference between H_{shift} and H_{SRTM}. (F) Histogram of the difference between H and H_{SRTM}.
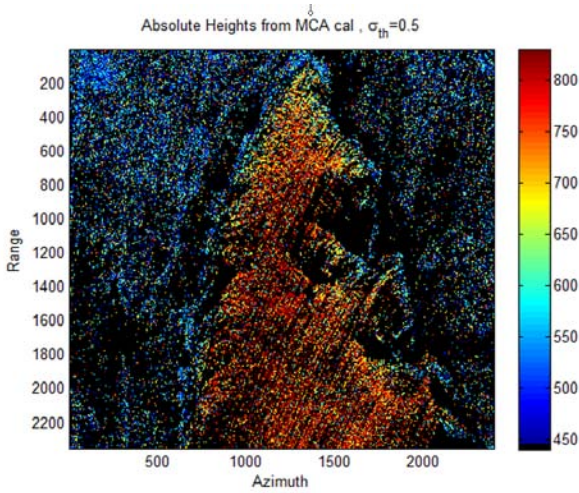
Figure 4. Final heights obtained after calibration. The constraint $\sigma_\Phi < 0.5$ was used to reject noisy pixels (sketched in black in the map).

Errors in orbital state vectors impact on the computation of geometrical parameters, which in turn are involved in the computation of both the reference ellipsoidal phase and the coefficient of phase-to-height conversion $\Phi 2H$. Hence, absolute measurements (both in phase and height) are strongly compromised unless either precise orbital parameters, or measurements on reference points, are available.

Thus a calibration is required to remove this offset. In the present case, the calibration procedure was performed by using the SRTM DEM. To make more robust the offset estimation, we used the H_{MCA} sketched in Fig. 3-(A), which was then strongly filtered to reduce noise.

Once the offset was estimated it could be used to compute the final heights map showed in Fig. 4. In this case we did not apply any spatial filtering, while the constraint $\sigma_\Phi < 0.5$ was used to reject noisy pixels (sketched in black in the map).

1. PARKFIELD TEST CASE

The MCA approach was also tested by processing CSK spotlight data acquired over an area around Parkfield (California, USA). The dataset appears well suited for MCA, since it consists of a tandem pair (reduced temporal decorrelation), with an extraordinarily wide bandwidth of 379 MHz. In Fig. 5, the footprint of the SAR acquisition is shown in yellow, superimposed over an optical image extracted from Google-Earth. The area enclosed by red borders was selected for the experiment, in view of both the variable topography and the surface coverage, consisting mainly of bare soil. The amplitude of the master image is also sketched on the bottom of the same figure. Relevant CSK parameters are listed on the right side of Tab. 1.
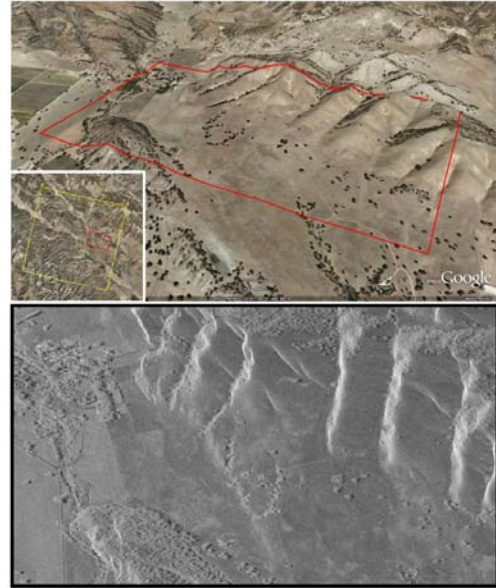

Figure 5. Parkfield test site. The area selected for the experiment is enclosed by red borders over an optical from Google-Earth. The amplitude of the master image for the test area is sketched on the bottom.

Also in this case, a DEM derived from SRTM mission is available on the same area and used for both calibration and validation.

A classical interferometric processing was performed at full band, then, the co-registered images were processed by using the MCA algorithm. 21 sub-look images were generated by splitting the full band using sub-bands of 50 MHz each, thus spanning a range of frequencies of about 320 MHz.

The slope map $C_1(x,y)$ was used, again, to compute both the absolute phase and the elevation map of the area. The absolute phase was computed through eq. (3) by taking into account also the contribution coming from the shift along range applied during co-registration. We filtered this absolute interferometric phase measurements using a mean filter, to derive a smooth continuous phase surface, with phase jumps from one pixel to its neighbour lower than half a cycle. This smoothed absolute phase was then wrapped modulo 2π, to compare the resulting interferogram to the original one. The two fringe patterns are shown in Fig.6-(A) and (B), respectively. Also in this case, they look similar.

To verify this statement, we used the smoothed absolute interferometric phase to flatten the classical interferogram. The result is shown in Fig.6-(C). Also in this case, the derived unwrapped interferometric phase allows flattening the classical interferogram, proving that this smoothed absolute phase surface is a correct unwrapped version of the classical interferogram within less than a cycle.

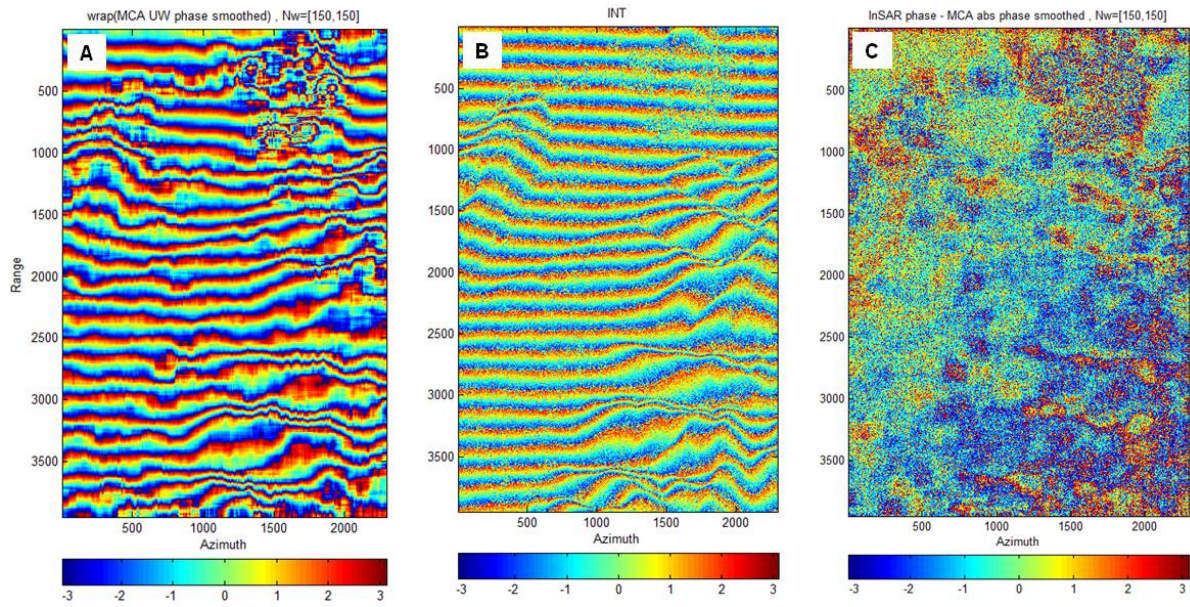The heights map was then computed by processing the absolute phase through eq. (4).

Figure 6. (A) Fringe pattern derived from the MCA-based absolute phase. (B) Fringe pattern of the full band interferogram. (C) Full band interferogram flattened by using the MCA-based absolute interferometric.
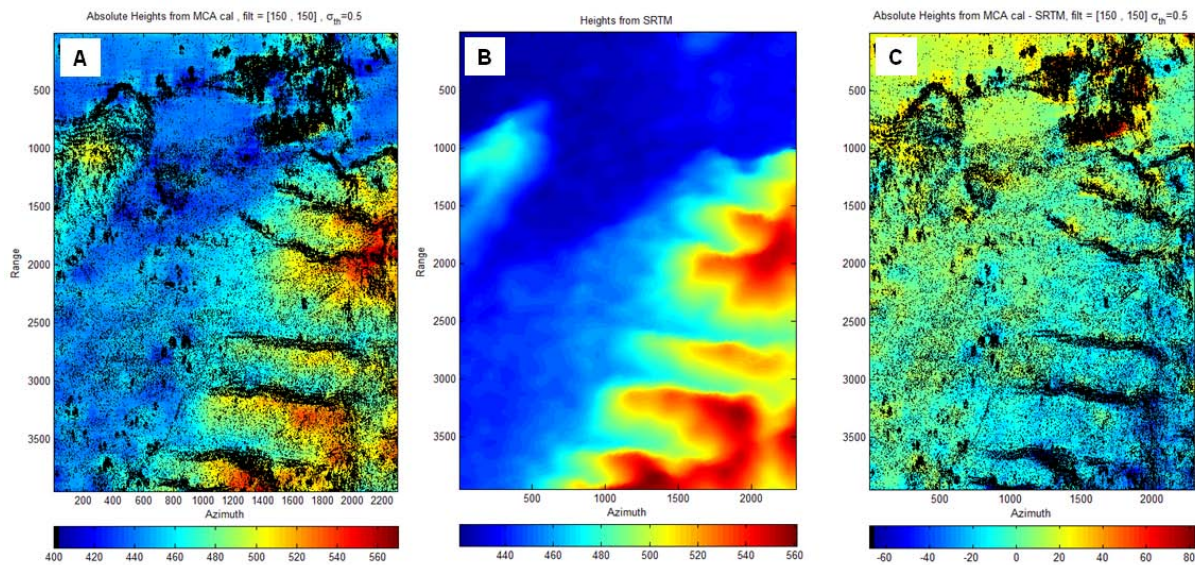

Figure 7. (A) Absolute heights after calibration. Noisy pixels were selected according to the constraint $\sigma_\phi < 0.5$ and represented in black in the map. (B) SRTM heights projected onto the SAR geometry (H_{SRTM}). (C) Difference between the map in inset (A) and the H_{SRTM} map.

Differently from the previous test case, the topographic reconstruction provided by using the co-registration shifts appears comparable with the reference DEM, apart from a global offset. This means that, in this case, the co-registration works properly. The histogram of the difference between H and H_{SRTM} shows a peak related to a global offset which was used to calibrate the result. Also in this case, the offset is related to atmospheric artefacts and/or orbital parameters inaccuracy. Fig. 7 shows the heights map H after calibration (inset A), the heights derived by resampling the SRTM DEM onto the SAR geometry (inset B), and their difference (inset C). Noisy pixels were selected according to the constraint $\sigma_\Phi < 0.5$, and are represented in black in the maps.

A residual phase trend is clearly present. It can be explained in terms of inaccuracies in the geometrical parameters used to compute the reference phase. Further investigations are being carried out.

2. CONCLUSIONS

This work presents the results of application of MCA to spaceborne SAR data acquired by both TSX and CSK data. Both datasets satisfy the processing requirements derived from the theoretical modelling provided in [2] . MCA was used to perform PU, as well as for absolute height measurement by using both TSX and CSK data.

An unwrapped phase surface was derived by strongly filtering MCA measurements. As already presented in [3] , we proved that this unwrapped phase surface is a valid approximation of the unwrapped interferometric phase, since it can be used to flatten the full-band interferogram. Application of MCA to CSK data was illustrated for the first time.

Concerning the absolute height retrieval on a pixel-by-pixel basis, we can conclude that it is possible, provided that orbital parameters are known with proper accuracy, and atmospheric contributions are negligible or compensated for. Otherwise, calibration procedures through independent measurements are required to fully determine the absolute heights. In the present test cases, height profiles were derived (from both TSX and CSK data) by using SRTM DEM to perform calibration. Moreover, we investigated the impact of coregistration on the MCA-based inference. For the TSX dataset acquired over the Ayers Rock monolith, where topography are particularly pronounced and

coregistration was not supported by DEM, MCA was able to correct (except for a bias) the height profile derived from the co-registration shift. In the case of the CSK dataset, due to the relatively regular topography and the DEM-assisted coregistration, the contribution of the MCA was less evident.

Further activities will be devoted to investigate the impact of the processing parameters on the MCA performances, to assess the precision of the height measurements, and to use the MCA for estimating atmospheric parameters.

REFERENCES

[1] N. Veneziani, F. Bovenga, A. Refice, "A wide-band approach to absolute phase retrieval in SAR interferometry", Multidimensional Systems and Signal Processing, MULT vol. 14(1-2), pp. 183-205, Kluwer Academic Publisher, 2003.

[2] F. Bovenga, V. M. Giacovazzo, A. Refice, N. Veneziani, R. Vitulli, "Multi-Chromatic Analysis of InSAR data: validation and potential", Proceedings of FRINGE 2009, ESRIN, Frascati, Italy, Nov.30 – Dec. 4, 2009.

[3] F. Bovenga, V. M. Giacovazzo, A. Refice, N. Veneziani, D. Derauw, R. Vitulli, "TSX meeting Interferometric Multi-Chromatic analysis OF TeRRASAR-X DATA", Proceedings of 4th TerraSAR-X Science Team Meeting, 14-16 February 2011, DLR – Oberpfaffenhofen.

[4] R. F. Hanssen, Radar Interferometry: Data Interpretation and Error Analysis. Dordrecht: Kluwer Academic Publishers, 2001.